Available online at www.sciencedirect.com
SCIENCE DIRECT®
PERGAMON
Polyhedron 22 (2003) 2227–2234
POLYHEDRON
www.elsevier.com/locate/poly

π–d Interaction-based molecular magnets

Akira Miyazaki [a,*], K. Okabe [a], K. Enomoto [a], J. Nishijo [a], T. Enoki [a], Fatima Setifi [b], Stéphane Golhen [b], Lahcène Ouahab [b], T. Toita [c], J. Yamada [c]

[a] Department of Chemistry, Tokyo Institute of Technology, 2-12-1 O-okayama, Meguro-ku, Tokyo 152-8551, Japan
[b] LCSIM, UMR-6511, Institut de Chimie de Rennes, Université de Rennes 1, 35042 Rennes Cedex, France
[c] Department of Material Science, Himeji Institute of Technology, 3-2-1 Kouto, Kamigori, Hyogo 678-1297, Japan

Received 7 October 2002; accepted 31 October 2002

Abstract

The crystal structures and physical properties of molecular magnets developed in our group are reviewed. (1) $(DMET)_2FeBr_4$ and its analogues are composed of alternating stacks of quasi-one-dimensional donor sheets and square lattice magnetic anion sheets. These salts undergo an SDW transition of the donor layer and an antiferromagnetic transition of Fe^{3+} spins on the anion layer. The one-to-one correspondence of the anomalies appearing on the magnetization curves and the magnetoresistance supports the presence of the π–d interaction. On applying pressure, a large negative magnetoresistance is observed for the all-sulfur compound $(EDTDM)_2FeBr_4$ in the marginal region of the SDW and metallic ground states. (2) (BDH-TTP)$[M(isoq)_2(NCS)_4]$ (M = Cr, Fe) show bulk weak ferromagnetism at 7.6 K. The donor cation radicals ($S = 1/2$) and anions ($S = 3/2$ (Cr), 5/2 (Fe)) form ferrimagnetic chains with close intermolecular S···S contacts, which are then antiferromagnetically coupled through the π–π overlap of the ligands and inter-chain S···S contacts of the donors. The non-collinear alignment of the molecular axes of adjacent anions is responsible for the canted spin structure.
© 2003 Elsevier Science Ltd. All rights reserved.

Keywords: Molecular conductor; Molecular magnet; π–d interaction; Magnetoresistance; Weak ferromagnetism; Magnetic anisotropy

1. Introduction

The hybridization of molecular metals and magnetic transition metal complexes gives an important feature to the physics and chemistry. When magnetic ions with d-electrons are introduced as a counterpart for organic donors having π-electrons, an exchange interaction defined as a π–d exchange interaction will be present between the donors and anions, and novel magnetic systems can be realized. Based on these viewpoints, we have developed a number of molecular magnets based on TTF-type derivatives, and investigated their electronic and magnetic properties in detail [1]. Such π–d interaction-based molecular magnets also attract many research groups to extend the fields of the molecule-based magnets [2].

These π–d interaction-based molecular magnets can be categorized into the following three groups based on the electronic nature of the donor side. In the first group, the organic π-electron system has an insulating ground state with no localized spins, due to the band insulating electronic structure, or instability inherent to the low-dimensionality (Peierls instability, charge-density wave). In this case, the localized moments of the d-electrons on the anions interacts with each other via the closed-shell donor π-electron system by means of super-exchange interaction. For example, a molecular weak ferromagnet $(C_1TET\text{-}TTF)FeBr_4$ (Fig. 1) is featured as a triangle-based ladder magnetic system, where the super-exchange interaction between the d-electron spins on magnetic anions is mediated by the π-electrons system of the donor molecules [3]. The second group is characterized as the organic-inorganic ferrimagnetic system, where the antiferromagnetic interaction between the $S = 1/2$ organic spins and $S > 1/2$ transition-metal complex spins leads to the bulk spin order. The origin of the localized moments on the donor sites can be strong

* Corresponding author. Tel.: +81-3-5734-2610; fax: +81-3-5734-2242.
E-mail address: miyazaki@chem.titech.ac.jp (A. Miyazaki).

0277-5387/03/$ - see front matter © 2003 Elsevier Science Ltd. All rights reserved.
doi:10.1016/S0277-5387(03)00178-5

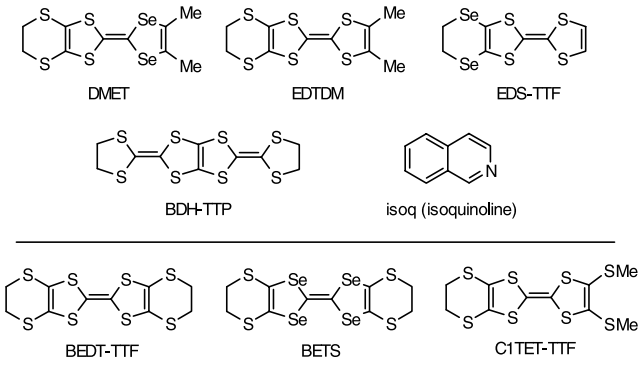

Fig. 1. Molecular structures of donor molecules; DMET (4,5-ethylenedithio-4′,5′-dimethyl-1,3-dithia-1′,3′-diselenafulvalene), EDTDM (4,5-ethylenedithio-4′, 5′-dimethyltetrathiafulvalene), EDS-TTF (4,5-ethylenediselenotetrathiafulvalene), BDH-TTP (2,5-bis(1,3-dithiolan-2-ylidene)-1,3,4,6-tetrathiapentalene), BEDT-TTF (bis(ethylenedithio)tetrathiafulvalene), BETS (bis(ethylenedithio)tetraselenafulvalene), and C_1TET-TTF (4,5-ethylenedithio-4′,5′-bis(methylthio)tetrathiafulvalene).

correlation between the π-electrons (Mott insulator, spin-density wave), or monovalent cationic nature of the donor molecules. The materials belonging to the third group can be described as 'conducting molecular magnets'. In this case, π-conduction carriers work to mediate the exchange interaction between the localized magnetic moments of d-electrons. This system is regarded as the molecular version of the ordinary inorganic metallic magnetic system with transition metals, where the exchange interactions between the spins are achieved through the s–d or s–f interaction. One of the representative works which can be classified in this category is λ-$(BETS)_2MCl_4$ (M = Fe, Ga) [4], where the $FeCl_4$ salt shows a π–d coupled antiferromagnetic state including field-induced superconductivity [5]. In every case, the essential point to define the π–d interaction-based molecular magnet is that the magnetic properties of the system cannot be described solely from the d-electron spins, and the contribution of the π-electron system is indispensable.

In this article, we report our recent results on the π–d interaction-based molecular magnets. In the next section $(DMET)_2FeBr_4$ and its isomorphous analogues $(EDTDM)_2FeBr_4$ and $(EDS\text{-}TTF)_2FeBr_4$ are discussed, where the presence of the π–d exchange interaction is directly proved by the comparison of its transport and magnetic properties including the giant negative magnetoresistance. We then discuss the molecular weak ferromagnets (BDH-TTP)[$M(isoq)_2(NCS)_4$], where the localized spins on the donor molecules mediates the spins on the transition metal complexes to realize the bulk weak ferromagnetism.

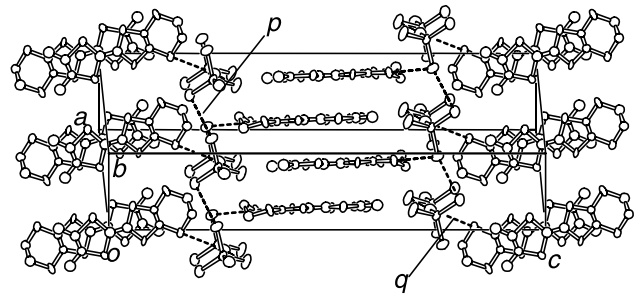

Fig. 2. Crystal structure of $(DMET)_2FeBr_4$ projected on the $[1\bar{1}0]$ plane. Dashed lines in the denote close intermolecular Br···Br (p) and Br···S (q) contacts.

2. Correlation of conductivity and magnetism through the π–d interaction in the salts D_2FeBr_4 (D = DMET, EDTDM and EDS-TTF)

As the asymmetric donor DMET is known to give metallic salts with various counter anions [6], we have focused on this donor molecule as the constituent of the organic part of the π–d interaction-based molecular magnets. In addition, since this molecule has three different chalcogen sites, the role of the π-electrons in the magnetic properties can be systematically investigated with the chalcogen substitution. According to these motivations, we have investigated the crystal structure, transport properties and magnetic properties of three radical ion salts with magnetic anions, $(DMET)_2FeBr_4$ [7], $(EDTDM)_2FeBr_4$ [8], and $(EDS\text{-}TTF)_2FeBr_4$ [9].

These salts have similar crystal structures as shown in Fig. 2. The donor molecules are stacked to form uniform one-dimensional columns. The columns located at $z \sim 0$ and $z \sim 1/2$ are extended along the $a+b$ and $a-b$ directions, respectively. The tetrahedral $FeBr_4^-$ anions form a distorted square lattice with Br···Br contacts, then interact with the donor sheets through intermolecular Br···S (or Br···Se) contacts, whose distances are summarized in Table 1. Due to the presence of these intermolecular contacts, not only the intra-layer interaction between the magnetic anions, but also the interlayer interactions through the π-electron system with considerable strengths are expected.

The conductivity of $(DMET)_2FeBr_4$ at room temperature (r.t.) is 15 S cm^{-1}, which is comparable to the other metallic DMET salts [6]. This salt shows a metallic conductivity, accompanied with a metal–insulator transition at $T_{MI} \sim 40$ K. This metal–insulator transition is also confirmed from the static susceptibility of the isostructural reference material with diamagnetic anion, $DMET_2GaBr_4$, which gives similar conduction behavior. Above T_{MI} the susceptibility shows Pauli paramagnetism, whereas below T_{MI} it shows a steep decrease, showing the disappearance of the conduction electrons. In the case of $(EDTDM)_2MBr_4$ (M = Fe, Ga), the in-plane resistivity shows metallic behavior above approximately 200 K and a gradual increase of the resistivity is observed below 200 K. However, this

Table 1
Structural and magnetic properties of $(DMET)_2FeBr_4$, $(EDTDM)_2FeBr_4$, and $(EDS\text{-}TTF)_2FeBr_4$

	$(DMET)_2FeBr_4$	$(EDTDM)_2FeBr_4$	$(EDS\text{-}TTF)_2FeBr_4$
Intermolecular contacts			
$d_{Br\cdots Br}$ (p) (Å)	3.88	3.87	3.86
$d_{Br\cdots S\ (Se)}$ (q) (Å)	3.76	3.74	3.49
Curie constant, C (emu K mol^{-1})	4.4	4.7	4.58
Weiss temperature, Θ (K)	−5.7	−2.8	−0.93
Néel temperature, T_N (K)	3.7	3.0	–
Spin flop field, B_{SF} (T)	2.0	1.8	–
Anomalies in the magnetization curve			
B_1 (T)	3.5	2.9	–
B_2 (T)	5.0	4.5	–

semiconducting behavior is an apparent one, since the magnetic susceptibility of $(EDTDM)_2GaBr_4$ shows Pauli paramagnetic behavior down to 15 K. An SDW transition then occurs at $T_{SDW} \sim 15$ K as evidenced by the presence of local magnetic moments from EPR and ^{13}C NMR [10] measurements. For the case of $(EDS\text{-}TTF)_2FeBr_4$, on the other hand, a metal–insulator transition occurs at approximately 250 K, below which semiconducting behavior with the activation energy $E_A = 380$ K is observed.

The magnetic susceptibility obeys the Curie–Weiss law in the high-temperature regime for these three salts. Their Curie constants C and the Weiss temperatures Θ are summarized also in Table 1. For the $(DMET)_2FeBr_4$ and $(EDTDM)_2FeBr_4$, antiferromagnetic transitions are observed at $T_N = 3.7$ and 3.0 K, respectively, whereas for $(EDS\text{-}TTF)_2FeBr_4$ no magnetic transition is observed above $T > 1.8$ K despite the presence of the close intermolecular Br···Se contacts (Fig. 3). The lack of magnetic interactions in $(EDS\text{-}TTF)_2FeBr_4$ can be explained as a consequence of the small contribution of the Se 4p orbital to the HOMO of the donor molecule. The magnetization curves of $(DMET)_2FeBr_4$ (Fig. 4(a)) and $(EDTDM)_2FeBr_4$ (Fig. 4(b)) measured at 1.8 K show spin-flop transitions at B_{SF} when the external field is applied parallel to the spin easy-axis ($=a$ axis). It should be noted that the easy-axis magnetization curve is beyond the hard-axis magnetization curve above the spin flop field B_{SF}, and has a shoulder around B_1. A similar shoulder is observed also for the hard-axis ($=b$-axis) magnetization curve around B_2. These anomalies more clearly appear as peaks on the dM/dB vs. B curves, i.e. field dependence of the magnetic susceptibilities. This unusual magnetic behavior cannot be explained in terms of only Fe^{3+} ($S = 5/2$) spins, strongly suggesting that the donor molecules importantly participate in the magnetic behaviors. In addition, the spin-flop field B_{SF} is almost unchanged between these two salts, while the anomalies at B_1 and B_2 appear at the lower field for the EDTDM salt. Since the main differences between these two salts are in the π-electron part, it is suggested that the anomalies at B_1 and B_2 are related to the participation of the donor in the magnetism.

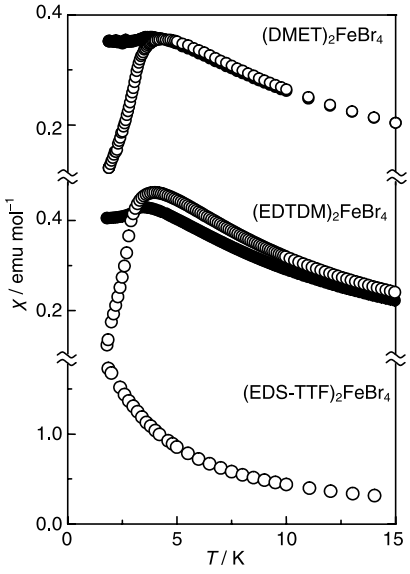

Fig. 3. Temperature dependence of the magnetic susceptibility of (a) $(DMET)_2FeBr_4$, (b) $(EDTDM)_2FeBr_4$, and (c) $(EDS\text{-}TTF)_2FeBr_4$, in a field of 1 T. Open circles: $B//a$-axis, filled circles: $B//b$-axis.

In order to confirm the contribution of the donor π-electron system in the magnetism, the magnetoresistance was measured for $(DMET)_2FeBr_4$ and $(EDTDM)_2FeBr_4$ by applying an external field along the a- and b-axes. Fig. 5 shows the field dependence of the in-plane magnetoresistance of $(DMET)_2FeBr_4$ measured at 1.6 K. A negative magnetoresistance is observed up to 15 T with a minimum appearing around 6 T. At the external field corresponding to B_{SF}, an anomalous kink is detected for the easy-axis ($//a$) direction. In addition, inflection points are also observed at B_1 and B_2 for the easy- and hard-axis direction, respectively, which are more clearly recognized on the $d(\Delta\rho/\rho)/dB$ vs. B plots. As there are clear one-to-one correspondences of the anomalies between the magnetoresistance (π-electrons)

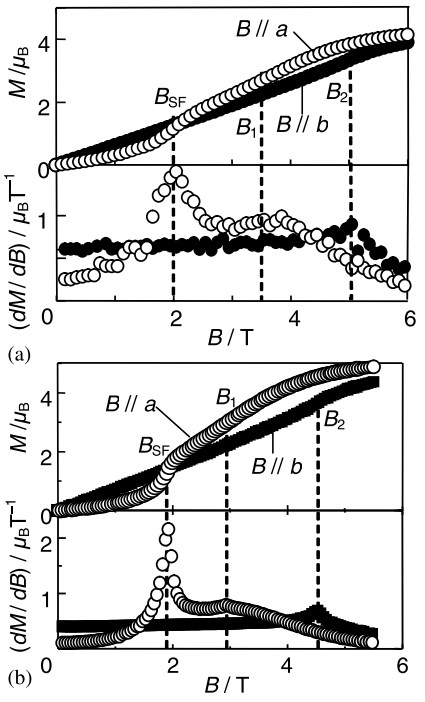

Fig. 4. Magnetization curves of (a) $(DMET)_2FeBr_4$ and $(EDTDM)_2FeBr_4$ at 1.8 K. Open circles: $B//a$-axis, filled circles: $B//b$-axis. Magnetic susceptibilities (dM/dB) are also plotted as a function of the field. B_{SF} denotes the spin-flop transition and B_1, B_2 show anomalies on the magnetization curves (see text).

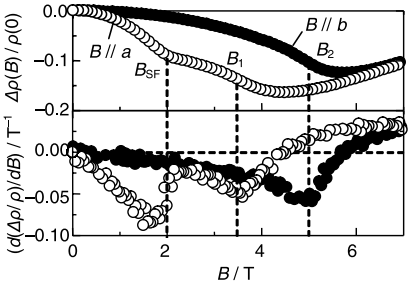

Fig. 5. Field dependence of the magnetoresistance of $(DMET)_2FeBr_4$ measured at 1.6 K for the in-plane ($\Delta\rho//(B)/\rho//(0)$) and out-of-plane ($\Delta\rho_\perp(B)/\rho_\perp(0)$) directions. Open circles: $B//a$-axis, filled circles: $B//b$-axis. The fields corresponding to the spin-flop transition (B_{SF}) and the anomaly (B_2) appearing on the magnetization curve are also indicated.

and magnetization (d-electrons), the presence of the π–d interaction is directly evidenced.

For $(EDTDM)_2FeBr_4$, application of hydrostatic pressure to the sample suppresses the increase of the resistivity in the low temperature range, which enables us to measure the magnetoresistance. Below $P \sim 0.92$ GPa the temperature dependence of the resistivity is similar to that at the ambient pressure, although the temperature for the resistivity minimum and the absolute value of the resistivity decrease as the pressure increases. When the pressure is above 0.92 GPa, the E_A (activation energy) vs. T plot shows an anomaly around 4 K (Fig. 6(a)), which is not observed in $(EDTDM)_2GaBr_4$ in the same pressure region. This anomaly rapidly disappears by further application of pressure. These results clearly show that the magnetic ordering of the localized d-electrons strongly affects the conducting π-electrons. Fig. 6(b) shows the field dependence of the magnetoresistance along the a-axis, under an external field parallel to the hard-axis ($//b$) at $T = 1.8$ K. The magnetoresistance of this $FeBr_4$ salt has negative values in the entire pressure and field ranges, whereas in the non-magnetic $GaBr_4$ salt only small positive magnetoresistance was observed. Therefore the origin of this large negative magnetoresistance is ascribed to the internal field of the $S = 5/2$ d-electron spins on the anions. The absolute value of the magnetoresistance increases with increasing field up to approximately 7 T and then saturated. Increasing pressure enhances the negative magnetoresistance below $P \sim 0.92$ GPa, at which the absolute value of the magnetoresistance takes a maximum. Above this pressure the absolute value of the magnetoresistance decreases with increasing pressure.

These results are understood as follows. In the low-field region, the localized d-electrons spins form an antiferromagnetic lattice that applies an internal field on the π-electron system. As the wavelength of this internal field from the d-electron system and SDW modulation on the π-electrons coincides, the SDW gap of the π-electron system is enhanced to produce the high-resistivity state. When a magnetic field is applied up to approximately 7 T, the magnetization of the localized moments on the $FeBr_4$ anions are saturated to form a

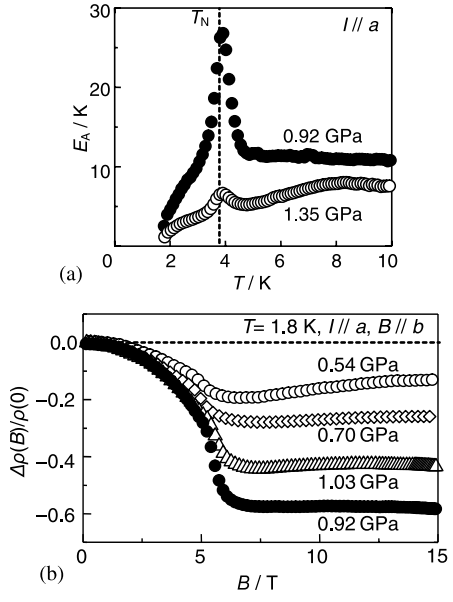

Fig. 6. (a) Temperature dependence of the activation energy for the resistivity of $(EDTDM)_2FeBr_4$ under hydrostatic pressures. (b) Field dependence of the magnetoresistance of $(EDTDM)_2FeBr_4$ under hydrostatic pressures. Currents and external magnetic fields are applied parallel to the a- and b-axes, respectively.

parallel spin arrangement. As a result, the periodicity of the internal field disappears, resulting in the free motion of the π-electrons within the organic conduction layer. This destabilization of the SDW state is prominent when the applied pressure is close to $P \sim 0.92$ GPa, where the electronic state of the π-electron system is situated on the boundary of the SDW and metallic states. Further increase of the pressure stabilizes the metallic system, which loses the sensitivity to the potential of the anion spins to reduce the negative magnetoresistance. Therefore the largest negative magnetoresistance at $P \sim 0.92$ GPa is the consequence of the sensitivity in the π-electron system to the applied field caused by the presence of the π–d interaction.

3. π–d interaction-based molecular weak ferromagnets (BDH-TTP)[M(isoq)$_2$(NCS)$_4$] (M = Cr, Fe)

For the realization of spontaneous magnetization in molecular magnets, the design of ferromagnetic interactions between the spins is first to be considered. However, the realization of a ferromagnetic interaction between the spins, by means of McConnell interactions [11] for example, is strongly dependent on the crystal structure, which is in general difficult to control. Alternatively, the combination of spins with different spin quantum numbers, i.e. the use of ferrimagnetic interactions, is a useful strategy, since the nearest neighboring exchange interaction in the ferrimagnetic chains is antiferromagnetic, which is easily established though intermolecular contacts such as coordination bonds. Based on this viewpoint, a large number of ferrimagnetic coordination polymers based on transition metal complex such as Mn(hfac)$_2$ (H$_2$hfac = hexafluoroacetylacetone) and stable organic radicals such as nitroxides have been extensively studied [12].

When the organic radicals are substituted by donor molecules, bulk magnetic materials with electrical conductivity will be expected. For this purpose we have adopted Reinecke salt-type complexes [M(isoq)$_2$(NCS)$_4$] (isoq = isoquinoline, M = Cr, Fe) as the inorganic part based on the following reasons. These transition-metal complexes have π-electron-based ligands (isoquinoline and thiocyanate), on which the d-electrons on the central metal are sufficiently delocalized. In fact, radical ion salts of these anions with BEDT-TTF show bulk weak ferromagnetic order [13], although the mechanism of the weak ferromagnetism has not been fully characterized. Here, we focused on a TTP-based donor BDH-TTP [14], as this donor has higher tendency of giving stable metals than BEDT-TTF. In this report, the magnetic properties of molecular weak ferromagnets (BDH-TTP)[M(isoq)$_2$(NCS)$_4$] (M = Cr, Fe) are discussed based on the results of single-crystalline magnetic susceptibility and ESR measurements [15].

The obtained salts are isomorphous regardless of the central metal of the magnetic counter anion. Fig. 7 shows the crystal structure of (BDH-TTP)[Cr(isoq)$_2$-(NCS)$_4$] projected on the *ac*-plane. The [M(isoq)$_2$-(NCS)$_4$] complex has a *trans* coordination, and the M–N distances of the axial isoquionoline ligands (M = Cr: 2.081(3), Fe: 2.161(3) Å) are slightly longer than that of the equatorial thiocyanate ligands (M = Cr: 1.988(3), Fe: 2.031(4) Å). Specifically, the MN_6 coordination octahedron is axially distorted along the *c*-direction. The terminal 1,3-dithiolane rings of the BDH-TTP cation have a conformational disorder due to their non-planarity. The donor molecules and the magnetic anions form one-dimensional uniform chains along the *c*-axis with remarkably close intermolecular S···S contacts (shortest distances: M = Cr: 3.264(2), Fe: 3.287(1) Å) between the TTP moieties of the donor molecules and thiocyanate ligands of the anions. These chains are then connected by a π–π overlap of isoquinoline ligands (arrows in the figure; interplanar distance: M = Cr: 3.597(5), Fe: 3.579(5) Å) and S···S contacts between the BDH-TTP cation radicals (not shown in the figure; M = Cr: 3.639(2), Fe: 3.664(2) Å). It is necessary to point out that the anions belonging to neighboring chains are not parallel, as they are related by the *c*-glide symmetry operation. The angle between the molecular axes (defined as isoq–M–isoq axes) is 5.5(3)° and 3.3(3)° for M = Cr and Fe, respectively.

Due to the 1:1 stoichiometry and alternate chain structure of donors and anions, these salts show poor electrical conductivities ($\sigma(300\ \mathrm{K}) = 10^{-5}\ \mathrm{S\ cm^{-1}}$). The magnetic susceptibility of both salts obeys the Curie–Weiss law above 50 K, and the Curie constant C and Weiss temperature Θ are estimated at $C = 2.19$ emu K mol^{-1}, $\Theta = -20.4$ K for the Cr salt, and $C = 4.95$ emu K mol^{-1}, $\Theta = -10.1$ K for the Fe salt. These Curie constants are close to the corresponding spin-only value

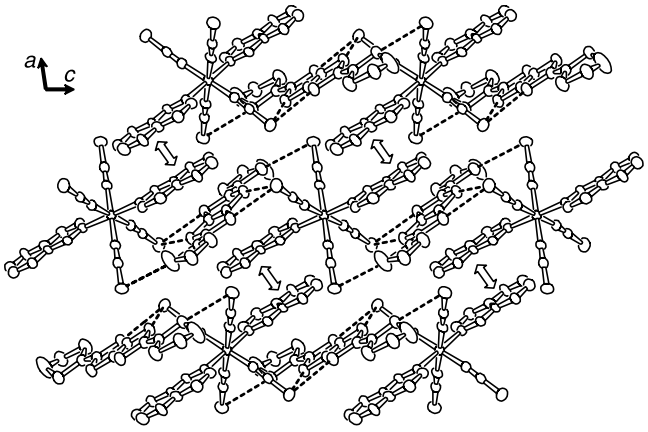

Fig. 7. Crystal structure of (BDT-TTP)[M(isoq)$_2$(NCS)$_4$] (M = Cr, Fe) projected on the *ac*-plane. Dashed lines are short intermolecular S···S contacts, and the arrows are π–π stacking between the isoquinoline ligands.

(M = Cr: 2.25, M = Fe: 4.75 emu K mol^{-1}) for non-interacting anion ($S = 3/2$ (Cr), 5/2 (Fe)) and donor ($S = 1/2$) spins. Negative Weiss temperatures (M = Cr: −20.4, Fe: −10.1 K) show the antiferromagnetic interaction between the donor spins and anion spins via intermolecular S···S contacts. Below 50 K the susceptibility deviates from the Curie–Weiss law, and shows a steep increase at $T_C = 7.6$ K for both salts due to a magnetic transition. Fig. 8(a) shows the temperature dependences of the magnetic susceptibility measured using a single crystal of (BDH-TTP)-[$Cr(isoq)_2(NCS)_4$]. Below $T_C = 7.6$ K a steep increase and decrease of the susceptibility are observed for $B//b$ and $B//c$, respectively. On the magnetization curves at $T = 2$ K (Fig. 8(b)), a small hysteresis loop is observed for $B//b$ with a remanent magnetization of $0.10\mu_B$ and a coercive field of 10 mT, whereas for $B//c$ a spin-flop transition is detected around $B = 1$ T. These results show that, in the magnetic ordered state, the donor spins and anion spins are ferrimagnetically coupled with the spin easy-axis along the c-axis, and that the contributions from the neighboring ferrimagnetic chains does not fully compensated by an inter-chain antiferromagnetic interaction to produce weak remanent magnetization along the b-axis. From the ratio of the remanent magnetization to the magnetization at $B = 5.5$ T (M = Cr: $2\mu_B$, Fe: $4\mu_B$), the spin-canting angle is estimated at 2.9° and 1.4° for M = Cr and Fe, respectively, which is comparable to the angles between the molecular axes of the anions.

The ESR spectra of both compounds give a single Lorentzian signal in the whole temperature range without separating the donor and anion spins, suggesting the presence of an exchange interaction between these two spin species. Fig. 9 show the temperature dependence of the g-value and the peak-to-peak linewidth of (BDH-TTP)[$Cr(isoq)_2(NCS)_4$]. The g-value at r.t. (average: 1.989) is close to the value of $K_3[Cr(CN)_6]$ (1.992) [16], showing that the observed ESR signal mainly comes from the d^3 Cr^{3+} spins. Below $T \sim 100$ K, the g-values gradually decrease for $B//a$, b and increase for $B//c$ as the temperature decreases. These results suggest the presence of short-range order of the spins above the magnetic transition temperature, caused by the low-dimensional nature of the ferrimagnetic chain [17]. The peak-to-peak line widths at r.t. ($B//a$: 15.8, $//b$: 10.4, $//c$: 16.2 mT) are smaller than the corresponding dipolar widths ($//a$: 47, $//b$: 43, $//c$: 67 mT) calculated for $S = 3/2$ anion spins and $S = 1/2$ donor spins, showing the effect of the exchange narrowing. The line width increases gradually as the temperature decreases below $T \sim 100$ K and shows a divergence as a precursor of a magnetically ordered state, consistent with the presence of the canted weak ferromagnetic state.

The spin structure below T_C can be schematically illustrated as in Fig. 10. The short S···S contacts between the donor and anion (solid lines in the figure) realizes the ferromagnetic alignment of the anion (S = 3/2 or 5/2) and donor ($S = 1/2$) spins within the chain. The adjacent chains are also connected via the π–π overlap of isoquinoline ligands (dotted lines) and the S···S contacts between the BDH-TTP cation radicals (dot-dashed lines), which can provide an inter-chain exchange path between the spins. As two adjacent anions are not parallel, the Dzyaloshinsky–Moriya interaction [18] between the adjacent magnetic anions must be considered as a candidate for the mechanism of the weak ferromagnetism. However, recent calculations based on the extended Hückel Hamiltonian [19] suggested that the donor–donor interaction mainly contributes to the inter-chain exchange interaction rather than the anion–anion exchange interaction, which shows that the canting of the magnetic anisotropy axes

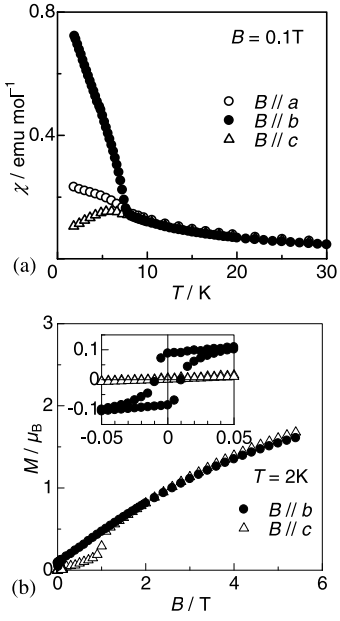

Fig. 8. (a) Temperature dependence of the magnetic susceptibility of (BDT-TTP)[$Cr(isoq)_2(NCS)_4$] measured at 0.1 T. (b) Magnetization curves measured at 2 K. Inset is an expanded view around $B = 0$.

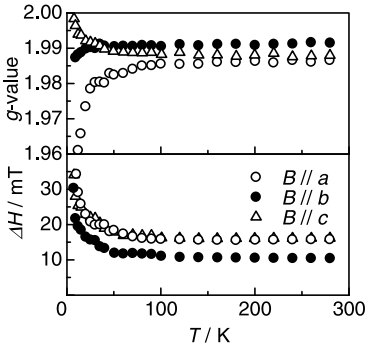

Fig. 9. Temperature dependence of the ESR g-values and peak-to-peak linewidth of (BDT-TTP)[$Cr(isoq)_2(NCS)_4$].

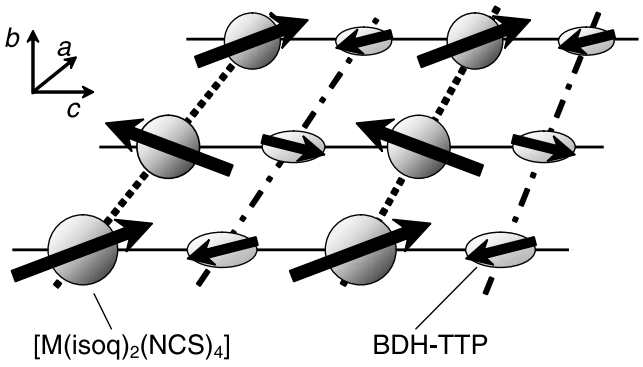

Fig. 10. Schematic drawing of the suggested spin structure of (BDT-TTP)[M(isoq)$_2$(NCS)$_4$] in the weak ferromagnetic phase.

of adjacent anions is a more plausible explanation for the weak ferromagnetic interaction between the ferrimagnetic chains.

4. Summary

We have developed molecular magnets based on organic donors and magnetic counter anions. (DMET)$_2$FeBr$_4$ and (EDTDM)$_2$FeBr$_4$ exhibit an antiferromagnetic order, where the magnetization curves show complex behavior, suggesting the contribution of the π-electrons on the donor layers. The interplay of the π-electrons on the donor side and the d-electrons on the anion side is directly shown by the coincidence of the anomalies on the magnetoresistance and magnetization curves. For (EDTDM)$_2$FeBr$_4$ large negative magnetoresistance is also observed, whose origin is explained in terms of the effect of the magnetic potential of the anion on the π-electrons of the donor via π–d interaction. The magnetic structure of (BDH-TTP)[M(isoq)$_2$(NCS)$_4$] is characterized as a spin-canted weak ferromagnetism, whose origin is explained as the non-parallel alignment of the magnetic anions between the ferrimagnetic alternate chains.

As mentioned above, organic complex-based molecular magnets based on organic donors and magnetic counter anions are found to be good targets for the development of molecular magnetism. The most important feature of these materials is the interplay of electrical transport and magnetic properties. When the π-electronic system on the donor molecules lies between metal and insulator phases, magnetic ordering of the anion layer strongly affects the transport properties on the donor layer to produce giant magnetoresistance as we have discussed, which draws attentions also from the viewpoints of application. On the other side, if the metallic π-electronic system is sufficiently stabilized, the localized d-electrons will interact with each other via free-electron-like conduction carriers to produce long-range interactions known as the Ruderman–Kittel–Kasuya–Yoshida (RKKY) interaction [20]. As this interaction has a spatially oscillatory behavior between ferromagnetic and antiferromagnetic states depending on the electronic state of the conduction electrons, a suitable design of organic and inorganic components will produce molecular ferromagnetic metal magnets, which is regarded as a one of the most challenging targets of molecular magnets.

Acknowledgements

We are grateful for Financial support from CNRS, CNRS-JSPS exchange program No. 9473 and NEDO research project 00MB4, and Grant-in-Aids (No. 12046231, 14540530) from the Ministry of Education, Science, Sports, and Culture, Japan. S.F. also thanks the French and Algerian Ministries of Education for a Ph.D. fellowship.

References

[1] (a) T. Enoki, J. Yamaura, A. Miyazaki, Bull. Chem. Soc. Jpn 70 (1997) 2005;
(b) A. Miyazaki, M. Enomoto, M. Enomoto, T. Enoki, G. Saito, Mol. Cryst. Liq. Cryst. 305 (1997) 425;
(c) T. Enoki, T. Umeyama, M. Enomoto, J. Yamaura, K. Yamaguchi, A. Miyazaki, E. Ogura, Y. Kuwatani, M. Iyoda, K. Kikuchi, Syn. Met. 103 (1999) 2275;
(d) A. Miyazaki, T. Umeyama, T. Enoki, E. Ogura, Y. Kuwatani, M. Iyoda, H. Nishikawa, I. Ikemoto, K. Kikuchi, Mol. Cryst. Liq. Cryst. 334 (1999) 379;
(e) A. Miyazaki, M. Enomoto, K. Enomoto, J. Nishijo, T. Enoki, E. Ogura, Y. Kuwatani, M. Iyoda, Mol. Cryst. Liq. Cryst. 376 (2002) 535.

[2] (a) T. Kominami, T. Matsumoto, K. Ueda, T. Sugimoto, K. Murata, M. Shiro, H. Fujita, J. Mater. Chem. 11 (2001) 2089;
(b) T. Naito, T. Inabe, K. Takeda, K. Awaga, T. Akutagawa, T. Hasegawa, T. Nakamura, T. Kakiuchi, H. Sawa, T. Yamamoto, H. Tajima, J. Mater. Chem. 11 (2001) 2221;
(c) L. Ouahab, Chem. Mater. 9 (1997) 109;
(d) E. Coronado, J.R. Galán-Mascarós, C.J. Gómez-García, V. Laukhin, Nature 408 (2000) 447.

[3] (a) M. Enomoto, A. Miyazaki, T. Enoki, Mol. Cryst. Liq. Cryst. 335 (1999) 293;
(b) M. Enomoto, A. Miyazaki, T. Enoki, Bull. Chem. Soc. Jpn 74 (2001) 459;
(c) M. Enomoto, A. Miyazaki, T. Enoki, Syn. Met. 121 (2001) 1800.

[4] (a) A. Kobayashi, T. Udagawa, H. Tomita, T. Naito, H. Kobayashi, Chem. Lett. (1993) 2179;
(b) H. Kobayashi, H. Tomita, T. Naito, A. Kobayashi, F. Sakai, T. Watanabe, P. Cassoux, J. Am. Chem. Soc. 118 (1996) 368;
(c) H. Kobayashi, A. Kobayashi, P. Cassoux, Chem. Soc. Rev. 29 (2000) 325.

[5] S. Uji, H. Shinagawa, T. Terashima, T. Yakabe, Y. Terai, M. Tokumoto, A. Kobayashi, H. Tanaka, H. Kobayashi, Nature 410 (2001) 908.

[6] (a) I. Ikemoto, K. Kikuchi, K. Saito, K. Kanoda, T. Takahashi, K. Murata, K. Kobayashi, Mol. Cryst. Liq. Cryst. 181 (1990) 185;
(b) K. Murata, K. Kikuchi, T. Takahashi, K. Kobayashi, Y.

Honda, K. Saito, K. Kanoda, T. Tokiwa, H. Anzai, T. Ishiguro, J. Mol. Elect. 4 (1954) 173.
[7] K. Enomoto, A. Miyazaki, T. Enoki, Syn. Met. 120 (2001) 977.
[8] (a) K. Okabe, K. Enomoto, A. Miyazaki, T. Enoki, Mol. Cryst. Liq. Cryst. 376 (2002) 513;
(b) K. Okabe, A. Miyazaki, T. Enoki, Syn. Met. 135 (2003) 693.
[9] A. Miyazaki, T. Enoki, Syn. Met. 133–134 (2003) 543.
[10] K. Kanoda, K. Miyagawa, private communication.
[11] H.M. McConnell, J. Chem. Phys. 39 (1910) 1963.
[12] H. Iwamura, K. Inoue, in: J.S. Miller, M. Drillon (Eds.), Magnetism: Molecules to Materials, vol. II (Chapter 2), Wiley-VCH, Weinheim, 2001.
[13] (a) S.S. Turner, C. Michaut, S. Durot, P. Day, T. Gelbrich, M.B. Hursthouse, J. Chem. Soc., Dalton Trans. (2000) 905;
(b) S.S. Turner, D. Le Pevelen, P. Day, K. Prout, J. Chem. Soc., Dalton Trans. (2000) 2739;
(c) F. Setifi, S. Golhen, L. Ouahab, S.S. Turner, P. Day, CrystEngCommun. 4 (2002) 1.
[14] J. Yamada, M. Watanabe, H. Anzai, H. Nishikawa, I. Ikemoto, K. Kikuchi, Angew. Chem., Int. Ed. 38 (1999) 810.
[15] F. Setifi, L. Ouahab, S. Golhen, A. Miyazaki, K. Okabe, T. Enoki, T. Toita, J. Yamada, Inorg. Chem. 41 (2002) 3786.
[16] J.M. Baker, B. Bleaney, K.D. Bowers, Proc. Phys. Soc. Sect. B 69 (1956) 1205.
[17] K. Nagata, Y. Tazuke, J. Phys. Soc. Jpn 32 (1972) 337.
[18] (a) I. Dzyaloshinski, J. Phys. Chem. Solids 4 (1958) 241;
(b) T. Moriya, Phys. Rev. 120 (1960) 91.
[19] M. Katsuhara, T. Mori, private communications.
[20] (a) M.A. Ruderman, C. Kittel, Phys. Rev. 96 (1954) 99;
(b) T. Kasuya, Prog. Theor. Phys. 16 (1956) 45;
(c) K. Yoshida, Phys. Rev. 106 (1957) 893.